AN X-RAY STUDY OF MAGNETIC FIELD STRENGTHS AND PARTICLE CONTENT IN THE LOBES OF FR II RADIO SOURCES

J. H. Croston,[1,2] M. J. Hardcastle,[2,3] D. E. Harris,[4] E. Belsole,[2] M. Birkinshaw,[2] and D. M. Worrall[2]

ABSTRACT

We present a *Chandra* and *XMM-Newton* study of X-ray emission from the lobes of 33 classical double radio galaxies and quasars. We report new detections of lobe-related X-ray emission in 11 sources. Together with previous detections, we find that X-ray emission is detected from at least one radio lobe in ∼75% of the sample. For all of the lobe detections, we find that the measured X-ray flux can be attributed to inverse Compton scattering of the cosmic microwave background radiation, with magnetic field strengths in the lobes between $0.3B_{eq}$ and $1.3B_{eq}$, where the value B_{eq} corresponds to equipartition between the electrons and magnetic field, assuming a filling factor of unity. There is a strong peak in the magnetic field strength distribution at $B \sim 0.7B_{eq}$. We find that more than 70% of the radio lobes are either at equipartition or electron dominated by a small factor. The distribution of measured magnetic field strengths differs for narrow- and broad-line objects, in the sense that broad-line radio galaxies and quasars appear to be further from equipartition; however, this is likely to be due to a combination of projection effects and worse systematic uncertainty in the X-ray analysis for those objects. Our results suggest that the lobes of classical double radio sources do not contain an energetically dominant proton population, because this would require the magnetic field energy density to be similar to the electron energy density rather than the overall energy density in relativistic particles.

Subject headings: galaxies: active — quasars: general — radiation mechanisms: nonthermal — X-rays: galaxies

Online material: color figure

1. INTRODUCTION

Detections of X-ray inverse Compton (IC) emission from components of radio galaxies have the potential to resolve long-standing questions about their particle content and magnetic field strength, because they allow direct measurements of electron energy density, unlike observations of radio synchrotron emission, where the electron density and magnetic field strength cannot be decoupled. This technique has been successfully used to measure magnetic field strengths in the hot spots and lobes of FR II (Fanaroff & Riley 1974) radio galaxies and quasars. Measurements of the internal energy density in relativistic electrons obtained from X-ray lobe detections can be used to constrain source dynamics and particle content by allowing a comparison of the internal pressure with the external pressure from X-ray–emitting hot gas (e.g., Hardcastle et al. 2002; Croston et al. 2004). This is particularly important in view of the continuing uncertainty about the dynamical status and confinement of FR II lobes (Hardcastle & Worrall 2000).

There are several possible sources of photons to be IC-scattered up to X-ray energies by the radio-synchrotron–emitting electron population. In hot spots, where the electron density is high, the dominant photon population comes from the radio emission itself; this is the synchrotron self-Compton (SSC) process (Hardcastle et al. 2004). However, in the lobes the density of synchrotron photons is much lower, so that the photon energy density from the cosmic microwave background typically dom-

inates over that from the radio synchrotron emission. In addition, the photon field from the nuclear source may be important in some sources (Brunetti et al. 1997). The *Chandra X-Ray Observatory* and *XMM-Newton* have allowed a number of detections of X-ray emission from lobes to be made. In many sources the lobes have been claimed to be near to equipartition (e.g., Hardcastle et al. 2002; Belsole et al. 2004; Croston et al. 2004; Bondi et al. 2004; Overzier et al. 2005), whereas in others significant electron dominance is claimed (e.g., Isobe et al. 2002; Comastri et al. 2003; Kataoka et al. 2003b). However, the results are dependent on the assumed electron energy spectrum and photon population characteristics. The unknown properties of the electron population at energies below those observable in the radio also introduce considerable uncertainty (e.g., Harris 2005). Differences in the methods used to separate thermal and nonthermal X-ray emission, and in the calculations of IC emissivity, can also be important, so that estimates from different authors are often not directly comparable. As yet there is no overall picture of the magnetic field properties of the FR II population.

The particle content in radio galaxies and quasars has been the subject of debate over several decades. There are arguments in favor of electron-proton jets, principally based on energy transport close to the active nucleus (e.g., Celotti & Fabian 1993); however, several independent arguments favor electron-positron jets (e.g., Wardle et al. 1998; Homan & Wardle 1999; Kino & Takahara 2004). IC studies can provide indirect information on the particle content on the large scale: although relativistic protons are not directly observable by this process, IC observations that are consistent with equipartition between the magnetic field and electron energy densities make it difficult to accommodate an energetically dominant population of protons in the lobes. Hardcastle et al. (2004) have already used this argument to suggest that hot-spot energetics are not dominated by protons, and Hardcastle et al. (2002) and Croston et al. (2004) have applied it

[1] Service d'Astrophysique, CEA Saclay, L'Orme des Merisiers, 91191 Gif-sur-Yvette, France; jcroston@discovery.saclay.cea.fr.

[2] Department of Physics, University of Bristol, Tyndall Avenue, Bristol BS8 1TL, UK.

[3] School of Physics, Astronomy and Mathematics, University of Hertfordshire, College Lane, Hatfield AL10 9AB, UK.

[4] Harvard-Smithsonian Center for Astrophysics, 60 Garden Street, Cambridge, MA 02138.

to individual FR II lobes; extending it to FR II lobes in general would be of considerable interest.

In this paper we use the *Chandra* archives (together with some *XMM-Newton* data) to compile a large sample of FR II radio galaxies and quasars with which to investigate the IC properties of lobes. Our approach differs from that of Kataoka & Stawarz (2005) in that we not only select sources with a known hot-spot, jet, or lobe emission, but also include sources whose extended components have not previously been detected in X-rays: this allows us to consider limits on the magnetic field strength, and gives us a much larger sample (as well as allowing us to make some new lobe detections). In § 4 we compare our results with theirs. Throughout the paper we use a cosmology in which $H_0 = 70$ km s^{-1} Mpc^{-1}, $\Omega_m = 0.3$, and $\Omega_\Lambda = 0.7$. Spectral indices α are the energy indices and are defined in the sense $S_\nu \propto \nu^{-\alpha}$.

2. SAMPLE AND DATA ANALYSIS

2.1. *Sample*

The sample was compiled from the list of 3C FR II radio sources for which public *Chandra* observations existed as of early 2004, which comprises 36 objects (Hardcastle et al. 2004). We also included four *XMM-Newton* observations of 3C radio galaxies for which detailed analysis of lobe-related emission has previously been carried out (Belsole et al. 2004; Croston et al. 2004). This gave a total sample size of 40 objects, which span a redshift range of ∼0.05–2. In Table 1 the full sample is listed, together with details of the observations and references to previously published work.

2.2. *X-Ray Analysis*

Nine of the sources in the sample have previous detections of lobe-related emission analyzed by workers including a subset of the present authors, with analysis based around the SYNCH code of Hardcastle et al. (1998a). Of the remaining objects, six have previously published detections of lobe-related X-ray emission. For consistency with the rest of our sample, we reanalyzed the data for those lobe detections that had not previously been analyzed using our code.

We extracted the *Chandra* archive data for the 31 objects not previously studied by our group and prepared and analyzed the data using standard methods using CIAO 3.1 and CALDB 2.28. The data were filtered for good time intervals, and an image in the energy range 0.5–5.0 keV was made for each source. We examined the X-ray image to determine whether it would be possible to make a measurement of the lobe-related X-ray emission. In seven cases, we decided that it would be impossible to determine accurately the level of X-ray emission associated with the radio lobes, either because of background-subtraction difficulties or because of other confusing components of X-ray emission. These cases were 3C 123, 3C 295, 3C 401, 3C 405, and 3C 438, which are all in rich clusters that in several cases show complex structure on the scales of the radio lobes; 3C 294, where extended non-thermal X-ray emission, not associated with the lobes, is present (Crawford et al. 2003); and 3C 324, where hot spot–lobe separation would be difficult (Hardcastle et al. 2004). In addition, there were several sources for which it was only possible to determine the level of lobe-related X-ray emission accurately for one of the two lobes, because of confusion with bright active galactic nucleus (AGN), jet, or hot-spot emission. The sources for which only one lobe could be studied are 3C 9, 3C 207, 3C 212, 3C 254, 3C 280, 3C 303, and 3C 321. In total, the analysis was carried out for 24 radio galaxies and quasars, which, together with the nine previously studied objects, gives a total sample of 54 lobes.

Spectral extraction regions were chosen on the basis of the extent of the radio structure, as determined using the 1.4 GHz radio maps (see the next section). The regions are circular, rectangular, or elliptical approximations to the extent of low-frequency radio emission. In all but two cases spectra were obtained separately for each radio lobe. Low-frequency radio maps were used, as they best represent the distribution of the electrons responsible for scattering CMB photons to X-ray energies. In most cases the lobe-related emission is of extremely low surface brightness, so that accurate background subtraction is crucial. In many cases there is also X-ray emission from a bright AGN and from the hot-gas environment. We therefore used local background regions at the same distance from the core as the source regions, so as to minimize the contamination, which is expected to be symmetrically distributed, and in particularly difficult cases (strong nuclear X-ray emission and small lobes) used point-spread function (PSF) modeling based on CHART[5] and MARX to verify the correctness of our extraction regions. Spectral extraction was carried out using the CIAO task `psextract`, which produces source and background spectra and response files (we compared our results with those obtained using weighted response files generated using the `acisspec` script for several representative sources and found no significant differences; we therefore chose to use the considerably faster `psextract` script). We used the energy range 0.5–5.0 keV for spectral analysis.

Where there were sufficient counts, the spectrum was grouped to a minimum of 20 counts per background-subtracted bin, and a power-law model was fitted to the extracted spectrum using XSPEC. In all cases Galactic N_H was assumed, using values from pointed observations or obtained with the N_H tool provided by NASA's High Energy Astrophysics Science Archive Research Center (HEASARC),[6] based on the measurements of Dickey & Lockman 1990. In the case of 3C 452, where subtraction of any thermal emission was difficult due to the radio-source morphology, we also fitted a two-component MEKAL plus power-law model. In the majority of cases, however, the total number of background-subtracted counts was too low to fit a spectrum or there was no detected X-ray emission above the 3 σ background level. In those cases, we assumed a power-law photon spectrum with $\Gamma = 1.5$ and used the measured count rate or upper limit from the 3 σ background level to determine the 1 keV flux density. Table 2 gives details of the spectral fits for those sources for which it was possible to fit the spectrum. In most cases an acceptable fit is obtained for $\Gamma = 1.5$, as expected for IC emission by radio-synchrotron–emitting electrons with the typical injection energy spectrum predicted from shock acceleration (e.g., Bell 1978). Table 3 gives the absorbing column density, number of counts, and flux density measurements for the other detected sources, and Table 4 gives upper limits for the remaining sources.

In total, of the 39 lobes analyzed, 23 were detected at the 3 σ level or above. In Figures 1 and 2 we show contour maps made from smoothed images for each of the sources with at least one lobe detection where the data are unpublished, or where the lobe detection has not previously been presented (3C 47, 3C 109, 3C 173.1, 3C 179, 3C 200, 3C 215, 3C 275.1, 3C 280, 3C 281, 3C 334, and 3C 427.1). Radio maps are shown in gray scale to illustrate the relation between radio and X-ray emission.

2.3. *Radio Data*

The electrons responsible for scattering CMB photons to X-ray energies have $\Gamma \sim 1000$, and so their radio emission is

---

[5] See http://cxc.harvard.edu/chart.
[6] See http://heasarc.gsfc.nasa.gov.

TABLE 1

The Sample of X-Ray–Observed FR II Radio Sources

Source	z	Type[a]	α_R[b]	OBS[c]	ObsID[d]	Date Observed	Duration[e] (s)	Reference
3C 6.1	0.8404	N	0.68	C	3009	2002 Oct 15	36,492	1
3C 9	2.012	Q	1.12	C	1595	2001 Jun 10	19,883	2
3C 47	0.425	Q	0.98	C	2129	2001 Jan 16	44,527	1
3C 109	0.306	B	0.85	C	4005	2003 Mar 23	45,713	1
3C 123	0.2177	E	0.70	C	829	2000 Mar 21	38,465	3
3C 173.1	0.292	E	0.88	C	3053	2002 Nov 6	23,999	1
3C 179	0.846	Q	0.73	C	2133	2001 Jan 15	9,334	4
3C 184	0.994	N	0.86	C	3226	2002 Sep 22	18,886	5[f]
3C 200	0.458	N	0.84	C	838	2000 Oct 6	14,660	
3C 207	0.684	Q	0.90	C	2130	2000 Nov 4	37,544	6
3C 212	1.049	Q	0.92	C	434	2000 Oct 26	18,054	7
3C 215	0.411	Q	1.06	C	3054	2003 Jan 2	33,803	1
3C 219	0.1744	B	0.81	C	827	2000 Oct 11	17,586	8
3C 220.1	0.61	N	0.93	C	839	1999 Dec 29	18,922	9
3C 223	0.1368	N	0.74	X	0021740101	2003 May 30	34,000	10[f]
3C 228	0.5524	N	1.0	C	2453	2001 Apr 23	13,785	
3C 254	0.734	Q	0.96	C	2209	2001 Mar 26	29,668	11
3C 263	0.652	Q	0.82	C	2126	2000 Oct 28	44,148	12[g]
3C 265	0.8108	N	0.96	C	2984	2002 Apr 25	58,921	13
3C 275.1	0.557	Q	0.96	C	2096	2001 Jun 2	24,757	14
3C 280	0.996	N	0.81	C	2210	2001 Aug 27	63,528	11
3C 281	0.602	Q	0.71	C	1593	2001 May 30	15,851	14
3C 284	0.2394	N	0.95	X	0021740201	2002 Dec 12	43,000	10[f]
3C 292	0.710	N	0.80	X	0147540101	2002 Oct 29	34,000	5[f]
3C 294	1.78	N	1.07	C	3207	2002 Feb 27	122,020	15[h]
3C 295	0.4614	N	0.63	C	2254	2001 May 18	90,936	16
3C 303	0.141	B	0.76	C	1623	2001 Mar 23	14,951	17
3C 321	0.096	N	0.60	C	3138	2002 Apr 30	47,130	1
3C 322	1.681	N	0.81	X	0028540301	2002 May 17	43,000	5[f]
3C 324	1.2063	N	0.90	C	326	2000 Jun 25	42,147	1
3C 330	0.5490	N	0.71	C	2127	2001 Oct 16	44,083	12[g]
3C 334	0.555	Q	0.86	C	2097	2001 Aug 22	32,468	
3C 351	0.371	Q	0.73	C	2128	2001 Aug 24	45,701	12[g]
3C 390.3	0.0569	B	0.75	C	830	2000 Apr 17	33,974	
3C 401	0.201	E	0.71	C	3083	2002 Jul 20	22,666	18
3C 403	0.0590	N	0.74	C	2968	2002 Dec 7	49,472	19[f]
3C 405	0.0590	N	0.74	C	360	2000 May 21	34,720	20
3C 427.1	0.572	E	0.97	C	2194	2002 Jan 27	39,456	
3C 438	0.290	E	0.88	C	3967	2002 Dec 27	47,272	
3C 452	0.0811	N	0.78	C	2195	2001 Aug 21	79,922	21

[a] The radio-source types are as follows: N is for narrow-line radio galaxies, B is for broad-line radio galaxies, E is for low-excitation radio galaxies, and Q is for radio-loud quasasr.

[b] The low-frequency radio spectral index (normally between 178 and 750 MHz).

[c] This column indicates whether the observation was with *Chandra* (C) or *XMM-Newton* (X).

[d] *Chandra* or *XMM-Newton* observing identification.

[e] Original live time.

[f] The authors' analysis methods are similar to those used in the current paper, so we do not reanalyze this observation.

[g] The authors' analysis methods are similar to those used in the current paper, but we repeat their IC calculations to take into account a different cosmology and low-energy electron cutoff.

[h] The authors argue that there is IC emission produced by scattering of CMB photons around this high-redshift source; however, the emission is not coincident with the lobes or any detected radio emission, so this is not an X-ray lobe detection by our definition.

References.—(1) Hardcastle et al. 2004; (2) Fabian et al. 2003; (3) Hardcastle et al. 2001; (4) Sambruna et al. 2002; (5) Belsole et al. 2004; (6) Brunetti et al. 2002; (7) Aldcroft et al. 2003; (8) Comastri et al. 2003; (9) Worrall et al. 2001 (10) Croston et al. 2004; (11) Donahue et al. 2003; (12) Hardcastle et al. 2002; (13) Bondi et al. 2003; (14) Crawford & Fabian 2003; (15) Crawford et al. 2003; (16) Brunetti et al. 2001; (17) Kataoka et al. 2003a; (18) Reynolds et al. 2005; (19) Kraft et al. 2005; (20) Wilson et al. 2000; (21) Isobe et al. 2002.

emitted at $\nu \sim 100$ MHz, assuming a typical magnetic field strength of 1.5 nT (1 nT = 10 μG). This is at the lower end of the observable radio region. It is therefore essential to use the lowest frequency radio maps available that have sufficient resolution to determine the extent of the radio emission and the radio spectrum of the lobes. We used the 178 MHz flux densities from the 3C and 3CRR catalogs, and obtained 1.4 GHz flux densities for each lobe using the best available maps.

For those sources where we did not have access to a 1.4 GHz radio map, we extracted archive VLA data (choosing a VLA configuration that samples the largest angular structure of each source, so as to include all of the source flux) and performed

TABLE 2
SPECTRAL FITS FOR X-RAY LOBE DETECTIONS WITH SUFFICIENT COUNTS

Source	Net Counts[a]	N_H[b] (cm^{-2})	Γ[c]	$S_{1\,keV}$[c] (nJy)	χ^2/dof
3C 47N................................	197	5.87×10^{20}	1.4 ± 0.4	3.6 ± 0.7	4.9/6
3C 47S	434	5.87×10^{20}	1.9 ± 0.2	10 ± 1	21/15
3C 215N..............................	109	3.75×10^{20}	1.4 ± 0.3	2.9 ± 0.4	1/3
3C 215S	119	3.75×10^{20}	1.5 ± 0.5	2.9 ± 0.5	2.9/3
3C 219N..............................	188	1.51×10^{20}	2.0 ± 0.3	9 ± 1	3.6/6
3C 219S	147	1.51×10^{20}	1.7 ± 0.5	7 ± 1	7/4
3C 265E..............................	142	1.90×10^{20}	1.9 ± 0.2	3.1 ± 0.3	1/5
3C 452 (model I)................[d]	2746	1.19×10^{21}	1.75 ± 0.09	37 ± 2	96/89
3C 452 (model II) ....[d]	2746	1.19×10^{21}	1.5 (frozen)	23 ± 4	87/88

NOTE.—Spectra were fitted in the energy range 0.5–5.0 keV.
[a] *Chandra* background-subtracted 0.5–5.0 keV counts in the lobe.
[b] Assumed Galactic hydrogen column density, frozen for the purposes of the fit.
[c] Errors in are the statistical errors, 1 σ for one interesting parameter.
[d] Two models were fitted to the 3C 452 data, as described in the text. Model II includes a thermal component with $kT = 0.6 \pm 0.3$ keV, consistent with the results of Isobe et al. (2002).

calibration and mapping using standard techniques in AIPS. Table 5 lists the radio maps used to determine the ratio of lobe flux densities and to define the X-ray spectral extraction regions.

1.4 GHz flux densities were measured using tvstat in AIPS. The entire extent of low-frequency radio emission was measured for each lobe, as the X-ray extraction regions were chosen using the same maps. The flux from any hot spots or jets was excluded. Then 178 MHz flux densities for each lobe were estimated by scaling the 3C or 3CRR flux densities based on the ratio between the 1.4 GHz flux densities for that lobe and the total 1.4 GHz flux densities from the lobes. Here we assume that the 178 MHz flux density is dominated by emission from the radio lobes, so that jet and hot-spot emission is not important at that frequency. This procedure also implicitly assumes that the low-frequency spectral indices are the same for both lobes of a given source. In general, this assumption has not been tested, but since we know the high-frequency spectral indices of the lobes in a given source are rarely very different (Liu & Pooley 1991), it seems unlikely that it is seriously wrong. We have verified that low-frequency lobe

spectral indices are similar where suitable data (e.g., 330 MHz radio maps) are available to us: the results of this investigation suggest that the inferred 178 MHz lobe flux densities are likely to be wrong by at most 20%, which would correspond to a systematic error in the predicted IC emission of around 10%.

3. SYNCHROTRON AND INVERSE COMPTON MODELING

We used the X-ray flux densities or upper limits given in Tables 2, 3, and 4, and radio flux densities at 178 MHz and 1.4 GHz obtained as described in § 2.3, to carry out synchrotron and IC modeling using SYNCH (Hardcastle et al. 1998a) for the sources not previously analyzed using this method. The radio lobes were modeled either as spheres, cylinders, or prolate ellipsoids, depending on the morphology of the low-frequency radio emission. As the angle to the line of sight is not well constrained for most of the sources, the source dimensions are the *projected*

TABLE 3
X-RAY FLUX MEASUREMENTS FOR DETECTED LOBES WITH INSUFFICIENT COUNTS FOR SPECTRAL FITTING

Source	Net Counts[a]	N_H (cm^{-2})	$S_{1\,keV}$ (nJy)
3C 9W........................	13	4.11×10^{20}	0.6 ± 0.3
3C 109N......................	70	1.57×10^{21}	1.5 ± 0.3
3C 109S	69	1.57×10^{21}	1.5 ± 0.4
3C 173.1N....................	17	5.25×10^{20}	0.6 ± 0.2
3C 179E......................	17	4.31×10^{20}	1.3 ± 0.4
3C 179W......................	9	4.31×10^{20}	0.7 ± 0.3
3C 200	35	3.69×10^{20}	1.6 ± 0.4
3C 207W......................	23	5.40×10^{20}	0.6 ± 0.2
3C 265W......................	46	1.90×10^{20}	0.7 ± 0.2
3C 275.1S	20	1.89×10^{20}	0.5 ± 0.1
3C 280W......................	18	1.25×10^{20}	0.2 ± 0.1
3C 281N......................	25	2.21×10^{20}	1.0 ± 0.3
3C 334N......................	36	4.24×10^{20}	0.9 ± 0.3
3C 334S	36	4.24×10^{20}	0.9 ± 0.2
3C 427.1S	14	1.09×10^{21}	0.3 ± 0.1

[a] *Chandra* background-subtracted 0.5–5.0 keV counts in the lobe. The 1 keV flux densities were determined by assuming a power law with $\Gamma = 1.5$, as described in the text.

TABLE 4
UPPER LIMITS ON THE UNABSORBED 1 keV FLUX DENSITY FOR THE NONDETECTED LOBES

Source	Net Counts[a]	N_H (cm^{-2})	$S_{1\,keV}$ (nJy)
3C 6.1N..........................	<14	1.75×10^{21}	<0.4
3C 6.1S	<15	1.75×10^{21}	<0.5
3C 173.1S	<17	5.25×10^{20}	<0.6
3C 212S	<42	4.09×10^{20}	<1.7
3C 220.1N......................	<40	1.93×10^{20}	<1.2
3C 220.1S	<35	1.93×10^{20}	<1.1
3C 228N........................	<12	3.18×10^{20}	<0.8
3C 228S	<11	3.18×10^{20}	<0.7
3C 254W........................	<16	1.75×10^{20}	<0.4
3C 275.1N......................	<11	1.89×10^{20}	<0.3
3C 281S	<20	2.21×10^{20}	<0.8
3C 303E	<23	1.60×10^{20}	<1.0
3C 321S	<43	4.10×10^{20}	<0.7
3C 390.3N......................	<86	3.74×10^{20}	<1.8
3C 390.3S	<124	3.74×10^{20}	<2.7
3C 427.1N......................	<16	1.09×10^{21}	<0.4

[a] The 3 σ upper limit of *Chandra* background-subtracted 0.5–5.0 keV counts. The upper limit 1 keV flux densities were determined by assuming a power-law model with $\Gamma = 1.5$, as described in the text.
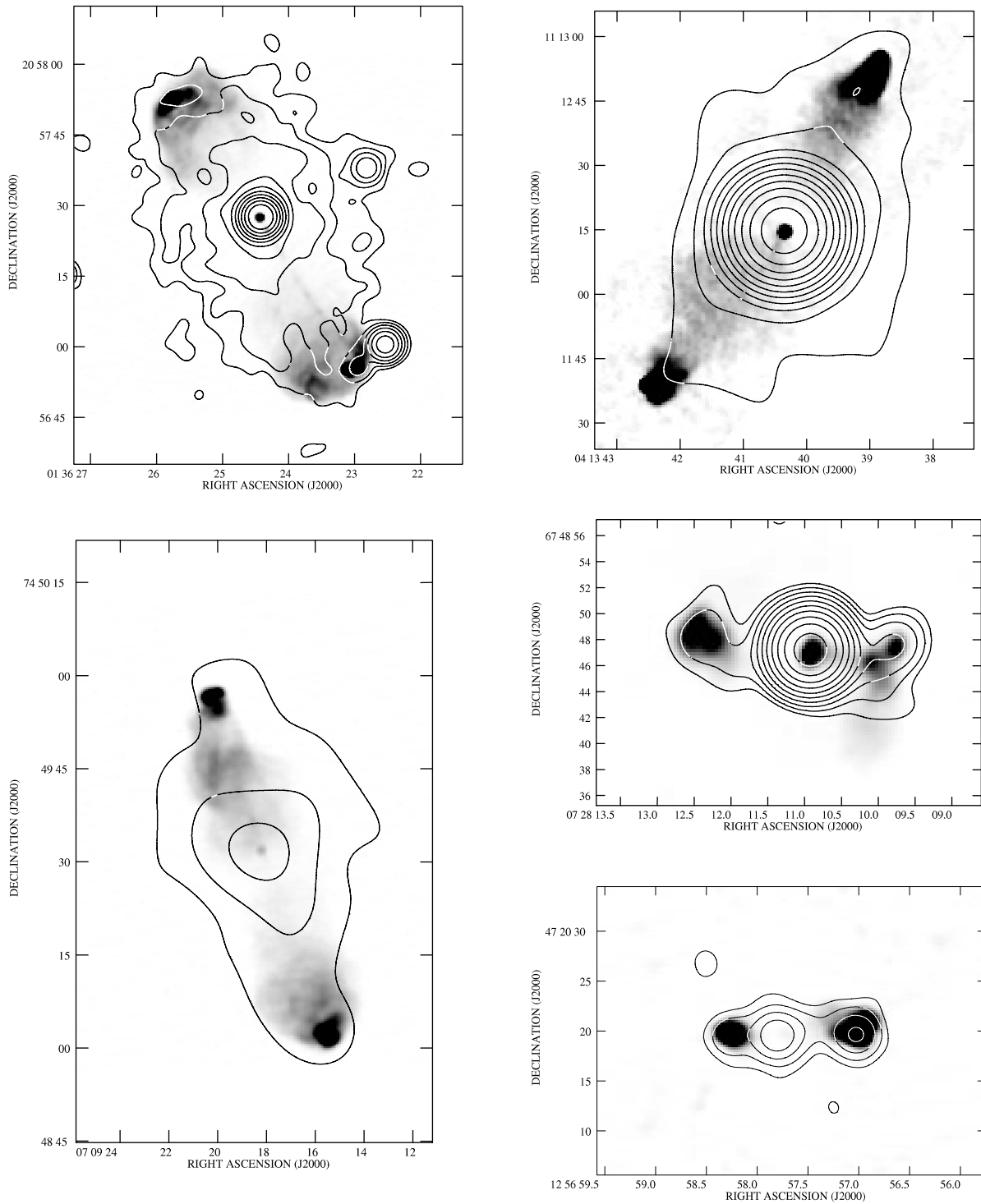
FIG. 1.—Contour maps from Gaussian smoothed 0.5–5.0 keV *Chandra* images of the X-ray emission from (*clockwise from top left*) 3C 47 ($\sigma = 1\farcs7$), 3C 109 ($\sigma = 4\farcs9$), 3C 179 ($\sigma = 1\farcs2$), 3C 280 ($\sigma = 1\farcs2$), and 3C 173.1 ($\sigma = 4\farcs4$). The X-ray contour levels are at 1, 2, 4, . . . × 3 σ level, calculated using the method of Hardcastle et al. (1998b). Radio maps shown in gray scale are from the 1.4 GHz radio maps listed in Table 5.

dimensions. This is not a good approximation, as sources in the sample will lie at all angles to the line of sight. We discuss the likely effects of this approximation later.

In each case we used the radio flux densities to normalize the synchrotron spectrum. We initially assumed a broken power-law electron distribution with initial electron energy index, δ, of 2, $\gamma_{min} = 10$ and $\gamma_{max} = 10^5$, and a break energy in the range $\gamma_{break} = 1200$–10,000, chosen so as to fit the two radio data points. In many cases the assumed spectral break (of 1 in electron

energy index) was not sufficiently large to fit the radio data. In these cases we instead lowered γ_{max} to fit the high-frequency slope of the radio spectrum. The effective γ_{max} is expected to decrease as the synchrotron plasma ages and/or expands, so this is a physically plausible change to make. The choice of γ_{max} does not significantly affect the prediction for CMB IC, as electrons with $\gamma \ll \gamma_{max}$ are responsible for the scattering to X-ray energies. (The prediction for SSC emission is significantly reduced if γ_{max} is reduced; however, SSC is not the dominant emission
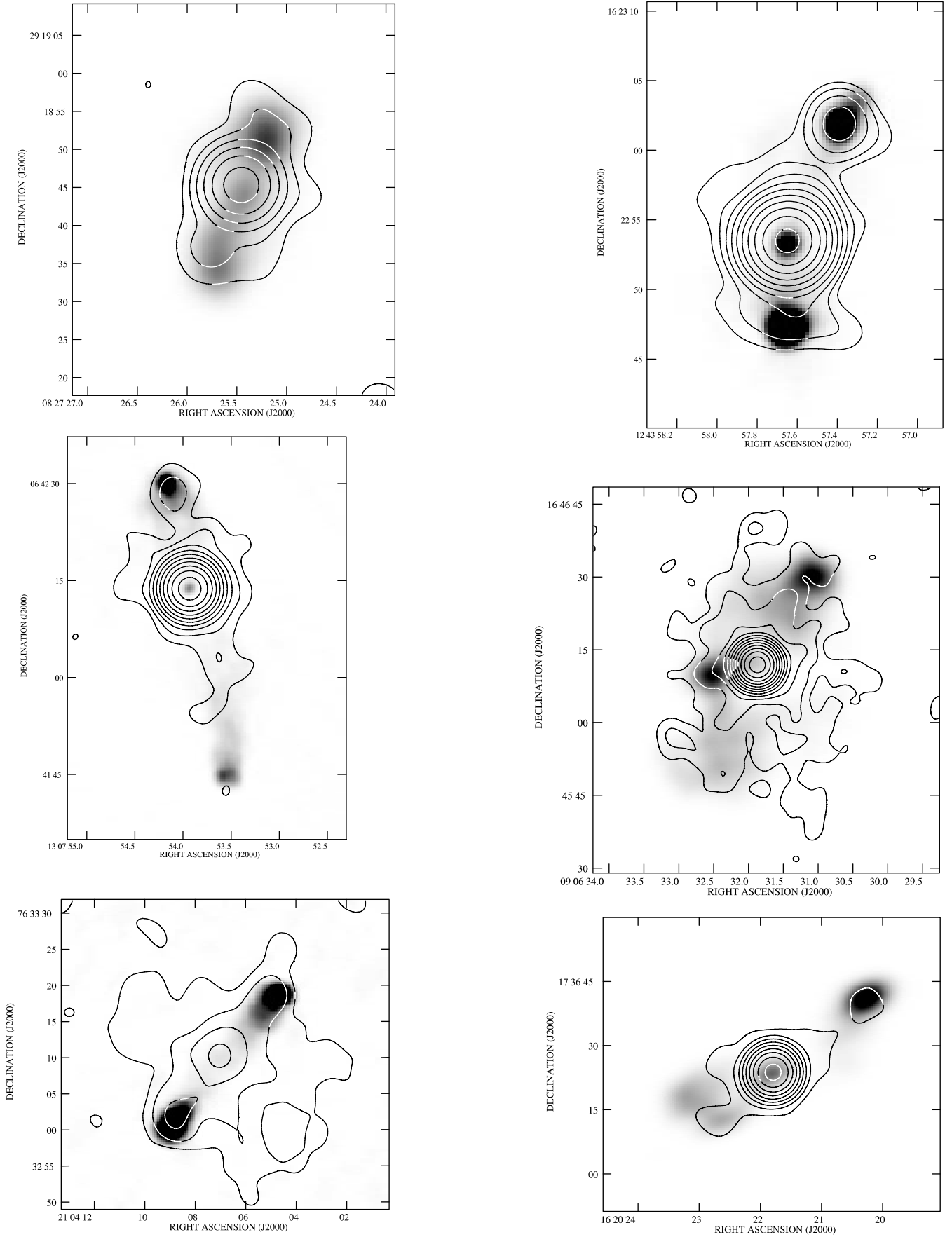
FIG. 2.—Contour maps from Gaussian smoothed 0.5–5.0 keV *Chandra* images of the X-ray emission from (*clockwise from top left*) 3C 200 ($\sigma = 2\rlap{.}''4$), 3C 275.1 ($\sigma = 1\rlap{.}''2$), 3C 215 ($\sigma = 1\rlap{.}''7$), 3C 334 ($\sigma = 2\rlap{.}''4$), 3C 427.1 ($\sigma = 1\rlap{.}''7$), and 3C 281 ($\sigma = 1\rlap{.}''7$). The X-ray contour levels are at 1, 2, 4, . . . $\times 3\,\sigma$ level, calculated using the method of Hardcastle et al. (1998b). Radio maps shown in gray scale are from the 1.4 GHz radio maps listed in Table 5.

TABLE 5
Radio Maps Used in the Analysis

Source	Frequency (GHz)	Date Observed	Reference/Proposal ID
3C 6.1	1.48	1987 Oct 3	AH291
3C 9	1.54	1992 Dec 13	AL280
3C 47	1.65		1
3C 109	1.45		2
3C 173.1	1.48		3
3C 179	1.65	1986 Mar 21	AC150
3C 200	1.49	1987 Nov 15	AH271
3C 207	1.54	1992 Dec 13	AL280
3C 212	1.66	1982 Mar 01	LAIN
3C 215	1.49	1987 Nov 15	AH271
3C 219	1.52		4
3C 220.1	1.40	1995 Oct 9	AH568
3C 228	1.42	1986 Jul 12	AL113
3C 254	1.56	1989 Feb 1	AB522
3C 265	1.42	1986 Jul 12	AL113
3C 275.1	1.49	1989 Jan 21	AP158
3C 280	1.56	1989 Feb 1	AB522
3C 281	1.43	1992 Nov 18	AB631
3C 303	1.45		3
3C 321	1.51	1986 Dec 2	AV127
3C 334	1.49	1986 Jul 12	AL113
3C 390.3	1.45		5
3C 427.1	1.54	1986 Jun 4	AL113
3C 452	1.41		1

Notes.—Observation dates are given for the archive data. References are given for published maps (where the electronic image was obtained from the 3CRR database; Leahy et al. 1998), and VLA proposal identifications for archive data.
References.—(1) Leahy et al. 1998; (2) Giovannini et al. 1994; (3) Leahy & Perley 1991; (4) Clarke et al. 1992; (5) Leahy & Perley 1995.

process in any of the sources.) The choice of parameters that affect the low-energy electron population (δ and γ_{min}) has a more important effect on the predicted IC flux. We therefore discuss the effect of modifying these parameters on our results and justify our adopted values in more detail in § 5.2. In Table 6 we give the parameters of the synchrotron model for each radio lobe.

We then determined the predictions for CMB IC and SSC at 1 keV based on the modeled synchrotron spectrum for each source, assuming equipartition between radiating particles and magnetic field and a filling factor of unity. For 3C 452, we adopted the 1 keV flux density from the two-component fit, which gave a better fit statistic than the single–power-law model. Table 7 gives the observed and predicted fluxes for each source in the sample, including the previously published sources.

4. RESULTS

To study the overall properties of the sample, we first constructed a histogram of R, the ratio of observed to predicted X-ray flux at equipartition. Figure 3 shows histograms of R for the detected and nondetected lobes. Note that $R = 1$ means that the CMB plus SSC model with an equipartition magnetic field and filling factor of unity can explain the observed X-ray flux. For $R > 1$, in an IC model, either the magnetic field is lower than the equipartition value, i.e., the lobes are electron dominated, or an additional photon field is present; $R < 1$ implies magnetic domination. We neglect here the effects of a filling factor of less than 1, which could be the case either for electrons, magnetic field, or both. If the electrons fill only a fraction of the lobe

TABLE 6
Synchrotron Model Parameters and Radio Spectral Information for Each Source

Source	γ_{max}	γ_{break}	Shape[a]	r[b] (arcsec)	S_{178}[c] (Jy)	$S_{1.4}$[d] (Jy)
3C 6.1N...........	3000	...	C	4.96	9.7	0.37
3C 6.1S	3000	...	C	4.22	5.2	0.2
3C 9W.............	3000	...	S	2.7	14.6	0.67
3C 47N............	6000	...	S	15	13.1	0.69
3C 47S	6000	...	S	17.96	15.7	0.83
3C 109N...........	4000	...	E	13	11.0	0.86
3C 109S	5000	...	E	13.6	12.5	0.98
3C 173.1N........	5000	...	E	8.34	9.4	0.83
3C 173.1S	6000	...	S	10.5	7.4	0.66
3C 179E..........	100000	3000	S	5.29	6.7	0.94
3C 179W..........	100000	3000	S	3.81	2.6	0.37
3C 200	100000	2000	S	13.3	12.3	1.52
3C 207W..........	3000	...	S	4.32	5.9	0.24
3C 212S	4000	...	S	3	0.07[e]	0.65
3C 215N...........	5000	...	S	13.5	7.3	0.41
3C 215S	6000	...	E	13.4	5.1	0.29
3C 219N...........	100000	4000	C	45.3	23.3	2.9
3C 219S	100000	3400	C	34.5	21.6	2.7
3C 220.1E........	100000	1200	S	11.1	8.0	0.86
3C 220.1W.......	100000	1200	S	9.7	9.2	1.0
3C 228N...........	100000	2000	C	7.02	9.6	1.3
3C 228S	100000	2000	C	7.36	14.2	1.9
3C 254W..........	2600	...	S	4.7	13.9	0.16
3C 265E..........	4000	...	C	9.3	11.9	0.33
3C 265W..........	5000	...	C	7.9	9.4	0.26
3C 275.1N........	2800	...	S	6.1	8.2	0.16
3C 275.1S	2800	...	S	5.35	11.7	0.23
3C 280W..........	2000	...	S	3.8	14.9	0.11
3C 281N...........	100000	1800	S	8.86	2.9	0.31
3C 281S	100000	1800	C	9.68	3.11	0.34
3C 303E..........	3000	...	S	9.3	12.2	0.39
3C 321W..........	5000	...	S	33.1	7.6	0.09
3C 334N...........	100000	2000	S	10.6	6.9	0.80
3C 334S	1000	1800	S	7.88	5.0	0.50
3C 390.3N........	6000	...	S	39	21.6	1.65
3C 390.3S	6000	...	S	48.3	30.2	2.3
3C 427.1N........	100000	2000	C	4.85	12.8	1.7
3C 427.1S	100000	2000	C	4.59	16.2	2.1
3C 452	100000	6000	C	88.96	59.3	10.5

Note.—In all cases γ_{min} is 10.
[a] Shapes are as follows: S = sphere, C = cylinder, and E = ellipsoid.
[b] Equivalent spherical radius of the modeled volume.
[c] Assumed 178 MHz radio flux density.
[d] Measured 1.4 GHz flux density.
[e] For this source it was not possible to use a 178 MHz flux density, because it was impossible to determine the flux ratio of the two lobes from the 1.4 GHz map (of very low resolution). We therefore used the 8 GHz flux density (given here) to constrain the spectrum instead.

volume with a uniform field, we will *underestimate R*, since the predicted CMB IC flux depends on the number density of electrons, which we will have overestimated. If there are strong magnetic field variations, but a uniform electron density, we will *overestimate R*, because our prediction for the number density and therefore CMB IC flux will be an underestimation. The effect of filling factor is discussed in more detail in Hardcastle & Worrall (2000).

Table 8 gives the measured and equipartition magnetic field strengths or upper limits and their ratio. We also list the ratio of electron to magnetic field energy densities, for comparison with other work in the literature. However, the electron and magnetic

TABLE 7
Observed and Predicted X-Ray Flux Densities at 1 keV for the IC Models

Source	1 keV Flux Densities (nJy)				R
	Observed	Predicted SSC	Predicted CMB-IC	Total Predicted	
3C 6.1N..............	<0.4	. . .	0.5	0.5	<0.8
3C 6.1S	<0.5	. . .	0.3	0.3	<1.7
3C 9W...............	0.6	. . .	0.7	0.7	0.9 ± 0.4
3C 47N...............	3.6	. . .	1.1	1.1	3.3 ± 0.6
3C 47S	10	. . .	1.6	1.6	6.3 ± 0.6
3C 109N..............	1.5	. . .	0.7	0.7	2.1 ± 0.4
3C 109S	1.5	. . .	0.8	0.8	1.9 ± 0.5
3C 173.1N...........	0.6	. . .	0.3	0.3	2.0 ± 0.7
3C 173.1S	<0.6	. . .	0.4	0.4	<1.5
3C 179E	1.3	0.04	0.4	0.4	3.3 ± 1
3C 179W.............	0.7	0.01	0.14	0.15	4.7 ± 2
3C 184N..............	0.2	0.103	0.051	0.154	1.3 ± 0.7
3C 200	1.6	0.02	1.2	1.2	1.3 ± 0.3
3C 207W.............	0.6	. . .	0.2	0.2	3 ± 1
3C 212S	<1.7	0.006	0.05	0.06	<28
3C 215N..............	2.9	. . .	0.7	0.7	4.1 ± 0.6
3C 215S	2.9	. . .	0.6	0.6	4.8 ± 0.8
3C 219N..............	9	0.02	3.3	3.3	2.7 ± 0.3
3C 219S	7	0.02	2.2	2.2	3.2 ± 0.2
3C 220.1E	<1.2	0.01	1.0	1.0	<1.2
3C 220.1W...........	<1.1	0.02	0.9	0.9	<1.2
3C 223N..............	3.1	0.004	1.3	1.4	2.2 ± 0.4
3C 223S	3.0	0.004	1.2	1.2	2.5 ± 0.4
3C 228N..............	<0.8	0.02	0.5	0.5	<1.6
3C 228S	<0.7	0.04	0.6	0.6	<1.2
3C 254W.............	<0.4	. . .	0.5	0.5	<0.8
3C 263NW...........	0.8	0.004	0.2	0.2	4.0 ± 1.0
3C 263SE............	0.5	0.001	0.1	0.1	5.0 ± 2.0
3C 265E	3.1	. . .	1.2	1.2	2.6 ± 0.3
3C 265W.............	0.7	. . .	0.8	0.8	0.9 ± 0.2
3C 275.1N...........	<0.3	. . .	0.4	0.4	<0.8
3C 275.1S	0.5	. . .	0.4	0.4	1.3 ± 0.3
3C 280W.............	0.2	. . .	0.6	0.6	0.3 ± 0.2
3C 281N..............	1.0	0.003	0.4	0.4	2.5 ± 0.8
3C 281S	<0.8	0.003	0.5	0.5	<1.6
3C 284E	1.9	0.003	0.93	0.94	2.0 ± 0.2
3C 284W.............	0.90	0.002	0.82	0.82	1.1 ± 0.2
3C 292	4.1	0.01	2.42	2.43	1.7
3C 303E	<1.0	. . .	0.3	0.3	<3.3
3C 321W.............	<0.7	. . .	1.0	1.0	<0.7
3C 322	1.4	0.05	1.3	1.4	1.0
3C 330NE	0.28	0.01	0.12	0.13	2.2 ± 0.8
3C 330SW...........	0.32	0.01	0.13	0.14	2.3 ± 0.6
3C 334N..............	0.9	0.01	0.7	0.7	1.3 ± 0.3
3C 334S	0.9	0.007	0.40	0.40	2.3 ± 0.5
3C 351N..............	1.1	0.001	0.15	0.15	7.3 ± 2.0
3C 351S	0.7	0.001	0.12	0.12	5.8 ± 2.5
3C 390.3N...........	<1.8	. . .	1.4	1.4	<1.3
3C 390.3S	<2.7	. . .	2.3	2.3	<1.2
3C 403E	1.63	0.002	0.35	0.35	4.6 ± 2.1
3C 403W.............	1.38	0.002	0.34	0.34	4.0 ± 2.1
3C 427.1N...........	<0.4	0.05	0.3	0.4	<1.0
3C 427.1S	0.3	0.08	0.3	0.4	0.8 ± 0.3
3C 452	23	0.4	7.8	7.8	2.9 ± 0.5

Notes.—Flux densities are predicted from the radio data on the assumption of equipartition using the SYNCH code as described in the text. Where no SSC flux density is quoted, the predicted value was less than 1 pJy, and so is irrelevant to the total IC flux density. R is the ratio of observed to predicted total 1 keV flux density. Errors on the R-value are entirely due to the uncertainties on the 1 keV flux densities, as quoted in this paper or the papers in which they were originally measured, and do not take into account any systematic uncertainties. For the sources where the spectral modeling details are not given in Table 6, the results are taken from the paper referred to in Table 1.
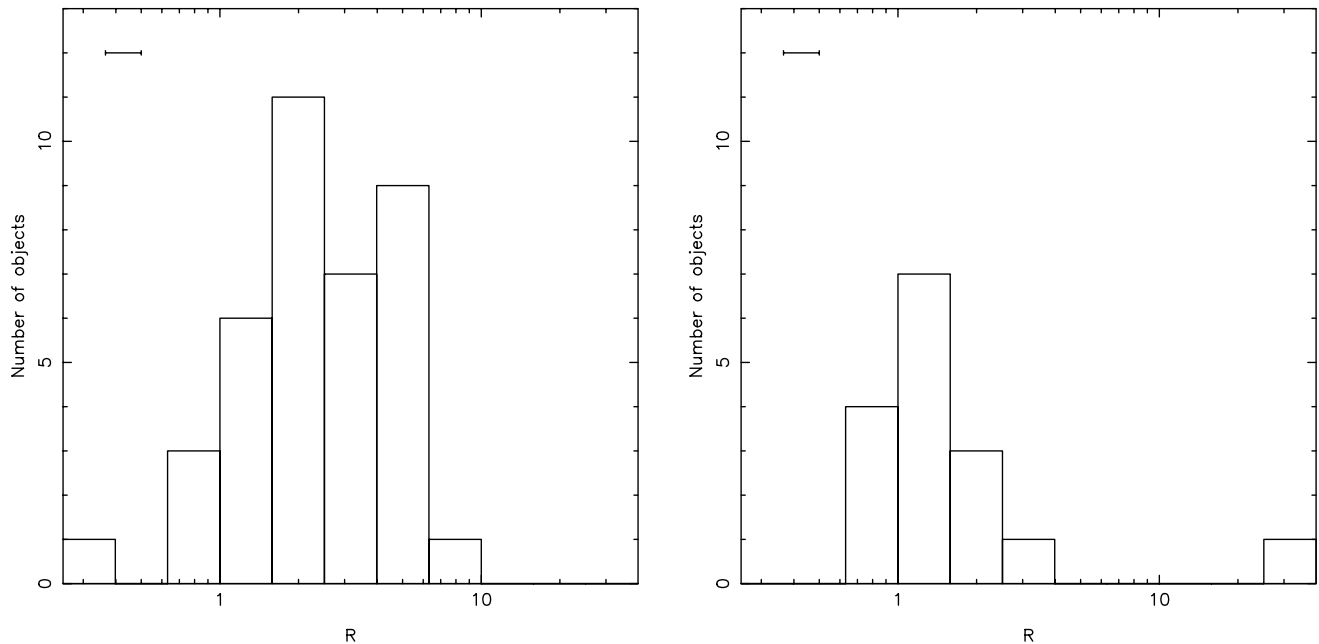
Fig. 3.—Distribution of R-values for the lobe sample. The left-hand plot shows the detected lobes, and the right-hand plot shows the upper limits for nondetected lobes. A representative error bar is shown in the top left-hand corner of the left-hand plot.

field energies are sensitive to small changes in magnetic field strength, so that the uncertainty on the value of U_e/U_b is large. We therefore consider R and B_{obs}/B_{eq} to be better measures of the departure from equipartition. For comparison with other results in the literature, we note that R relates to the two other commonly used measures of the departure from equipartition as $(B_{obs}/B_{eq}) \propto R^{-2/\delta+1}$ and $(U_e/U_b) \propto R^{\delta+5/\delta+1}$, where δ is the electron energy index ($2 \leq \delta \leq 3$).

The distribution of R-values for the detected sources is quite narrow, with the most extreme values being 0.3 and 7.3 (U_e/U_b ranges from 0.2 to 53). The majority of the sources have $R > 1$ and appear to be distributed around a peak at $R \sim 2$. However, the upper limits, in addition to the one detected source with $R < 1$, show that some FR II radio lobes could be magnetically dominated by at least a factor of 2 (or have a strongly structured magnetic field). Since the nondetections are only a small fraction of the sample, we can conclude that more than 36/54 lobes, or $\sim$70% of FR II radio galaxies and quasars if our sample is representative, are either at equipartition or electron dominated.

We next examined whether the type of radio source affects the observed R-value, by comparing the distributions of R for narrow-line radio galaxies and for broad-line objects (broad-line radio galaxies and radio-loud quasars). In the widely accepted unification model for radio galaxies and radio-loud quasars (e.g., Barthel 1989; Urry & Padovani 1995), these two categories of source, which possess different optical properties but similar radio structure, are thought to be the same objects seen at different angles to the line of sight. The narrow-line objects are thought to occupy angles between $45°$ and the plane of the sky, whereas the radio-loud quasars and broad-line radio galaxies occupy angles between $45°$ and the line of sight, with the difference in optical properties resulting from the presence of a torus of cold material along our line of sight to the narrow-line objects, which obscures the AGNs in those sources. We excluded the (few) low-excitation objects (Laing et al. 1994) from our comparison to avoid confusion. Figure 4 shows a histogram with the two categories of source indicated (only detected lobes are included; however, the fractions of nondetections in the two

subsamples are similar). It is immediately apparent that the distributions of R differ, in the sense that broad-line objects typically have higher values of R. The broad-line objects nearly all have $R > 2$, whereas the narrow-line objects mainly have $R < 2$. The median values of the samples are 2.1 (narrow-line) and 3.1 (broad-line). A median test rejects the hypothesis that the two subsamples have the same median with $\sim$92% probability.

One likely explanation for this marginally significant difference is the effect of projection on the volumes of the lobes. The predicted X-ray flux from CMB IC is proportional to the product of lobe volume and electron density. The electron density scales as $V^{-4/7}$ (Hardcastle et al. 2004), so that the predicted X-ray flux $S_{cmb} \propto V^{3/7}$. Since we have not taken projection effects into account, this means that for most sources we have underestimated the source volume and therefore S_{cmb}, so that R for a given source will be likely to be overestimated. The effect will be at its most severe for the broad-line radio galaxies and quasars, thought to be within $45°$ of the line of sight, where the volumes will have been significantly underestimated. If we assume that the population of narrow-line radio galaxies occupies all angles between $45°$ and the plane of the sky with equal probability, then the most probable angle at which to observe a narrow-line radio galaxy is at $\sim$70°, where R will be overestimated by a factor of $\sim$1.06, assuming that volume scales as l, where l is the observed lobe length. Similarly, assuming that the population of broad-line radio galaxies and quasars occupies all angles between $45°$ and the line of sight with equal probability, then the most probable angle at which to observe a broad-line radio galaxy or quasar is at $\sim$30°, where R will be overestimated by a factor of $\sim$1.34. (Note that for angles of less than $5°$–$10°$, R can be overestimated by a factor of $>$2.) These results show that the difference in the medians of the two samples cannot entirely be explained by a model in which the intrinsic value of R is the same for all radio galaxies and quasars.

To investigate this further, we carried out Monte Carlo simulations to examine whether a narrow distribution of intrinsic R-values could produce the observed distribution in R as a result of projection effects. We simulated samples of 10^6 radio galaxies

TABLE 8
MAGNETIC FIELD STRENGTHS AND CONTRIBUTIONS TO ENERGY DENSITY

Source	B_{eq}[a] (nT)	B_{obs}[b] (nT)	B_{obs}/B_{eq}[c]	U_e/U_B[d]
3C 6.1N	3.5	>3.5	>1.0	<1
3C 6.1S	3.4	>2.5	>0.74	<3
3C 9W	10.0	11.0	1.1	0.70
3C 47N	1.2	0.6	0.5	15
3C 47S	1.1	0.4	0.36	53
3C 109N	1.3	0.85	0.71	5
3C 109S	1.3	0.85	0.71	5
3C 173.1N	1.8	1.2	0.67	4
3C 173.1S	1.3	>1.0	>0.77	<3
3C 179E	2.9	1.3	0.45	<19
3C 179W	2.9	1.1	0.38	37
3C 200	1.4	1.1	0.79	3
3C 207W	3.2	2.0	0.63	6
3C 212S	7.4	>1.0	>0.14	<177
3C 215N	1.2	0.6	0.5	13
3C 215S	1.0	0.45	0.45	25
3C 219N	0.6	0.35	0.58	6
3C 219S	0.7	0.4	0.57	8
3C 220.1E	1.7	>1.7	>1	<1
3C 220.1W	1.9	>1.9	>1	<1
3C 223N	0.35	0.22	0.63	5
3C 223S	0.37	0.20	0.54	9
3C 228N	2.3	>1.8	>0.78	<2
3C 228S	2.4	>2.4	>1	<1
3C 254W	3.9	>3.9	>1.0	<1
3C 265E	2.1	1.3	0.62	7
3C 265W	2.3	2.3	1.0	1
3C 275.1N	2.5	>2.8	>1.1	<0.7
3C 275.1S	3.1	2.8	0.9	1
3C 280	5.5	9.0	1.6	0.2
3C 281N	1.4	0.9	0.64	6
3C 281S	1.4	>1.0	>0.71	<3
3C 284E	0.52	0.40	0.76	3
3C 284W	0.48	0.48	1.0	1
3C 303E	1.9	>0.9	>0.47	<15
3C 321W	0.60	>0.7	>1.2	<0.6
3C 334N	1.5	1.5	1	1
3C 334S	1.8	1.1	0.61	6
3C 390.3N	0.7	>0.7	>1	<1
3C 390.3S	0.7	>0.7	>1	<1
3C 403N	0.5	0.2	0.40	27
3C 403S	0.5	0.2	0.40	23
3C 427.1N	3.3	>3.3	>1	<1
3C 427.1S	3.7	3.7	1	1
3C 452	0.5	0.25	0.50	9

NOTE.—1 nT = 10 μG.
[a] Equipartition magnetic field strength.
[b] Magnetic field strength inferred from the level of X-ray flux.
[c] Ratio of observed to equipartition field strength.
[d] The ratio of electron energy density to magnetic field energy density.
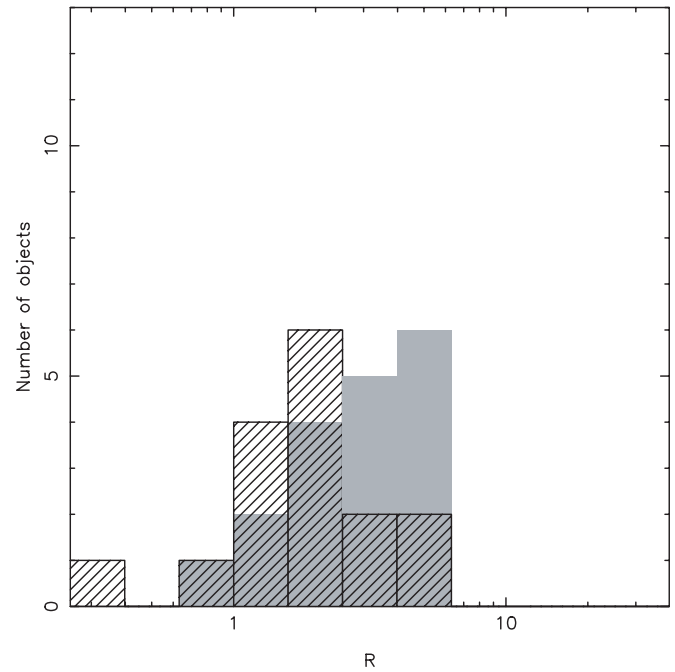

FIG. 4.—R-distribution for the narrow- and broad-line objects. The distribution for broad-line radio galaxies and quasars is indicated with filled rectangles, and that for narrow-line radio galaxies is overplotted in hatched rectangles. [*See the electronic edition of the Journal for a color version of this figure.*]

and quasars, distributed at angles to the line of sight with a probability distribution $P\theta\,d\theta = \sin\theta\,d\theta$ (i.e., based on the assumption that the lobes are randomly oriented with respect to the plane of the sky), and having an intrinsic Gaussian distribution of R with a mean $\langle R \rangle$ and variance σ. We then determined the *observed* R for each simulated source, taking into account projection [$R_{app} \propto (\sin\theta)^{-3/7}$], assuming cylindrical lobes (with $V \propto l$). We compared the simulated distribution of R_{app} to the observed distribution using a K-S test and found that the intrinsic values for $\langle R \rangle$ and σ that give the best match to the observed data are 2.5 and 1.15, respectively. We next tested whether the ob-

served distributions of R for the narrow- and broad-line objects could separately be explained by this intrinsic distribution. We find that the broad-line objects have a ∼40% probability of being drawn from a parent population having this intrinsic distribution; however, the narrow-line objects have only a ∼3% chance of being drawn from such a population. The intrinsic distribution that gives the best fit to the narrow-line objects alone has $\langle R \rangle = 1.7$ and $\sigma = 1.25$ (observed values of R for the narrow- and broad-line subsamples are 2.1 ± 1.1 and 3.2 ± 1.0, respectively).

We therefore conclude that projection is likely to be important in explaining the distribution of observed R-values; however, some additional explanation may be needed to explain the differences between the narrow- and broad-line objects. We note, however, that the *actual* distribution of inclination angles in this sample is unknown; it is clear from the fact that it contains roughly equal numbers of narrow- and broad-line objects that the probability distribution of line-of-sight angle we used for the simulation does not accurately represent the actual distribution in our sample. It is also possible that the high-redshift quasars (which often have high R-values) may be biased toward small angles to the line of sight, since the radio flux observed at 178 MHz in the highest redshift objects may have contributions from beamed components (although this will also reduce the intrinsic radio flux, which will act in the opposite direction to raise the observed value of R). Another possibility is that the systematic uncertainties in the X-ray analysis may be worse for the quasars, as contamination from the bright central source will be harder to remove; this could be compounded by the fact that the quasars are typically more distant and so have smaller angular sizes (although we find no correlation between R and angular size).

Hardcastle et al. (2004) carried out a similar analysis to that presented here for the X-ray properties of hot spots in FR II radio sources. They found that hot spots exhibit a large range in R-values, up to $R \sim 1000$, and concluded that a second X-ray emission component due to synchrotron radiation must be present in some hot spots. In this analysis we find that the IC model

can explain all X-ray lobe detections, with magnetic field strengths ranging from a fifth of the equipartition value to slightly higher than the equipartition value. This is unsurprising, as there is no known efficient acceleration mechanism in the lobes that can produce electrons of X-ray synchrotron–emitting energies, whereas electrons at the hot spots could be shock-accelerated to the energies required for X-ray emission. Hardcastle et al. also find that R is correlated with radio luminosity, so that the highest R-values are found in the weakest radio sources; they interpret this as being caused by a luminosity-dependent cutoff in the maximum energy to which the electrons are accelerated at the hot spot. We find no correlation between R and radio luminosity for the radio lobe sample. There is also no correlation between R and redshift. Finally, there is no correlation between the lobe R-values and the hot-spot R-values for the same sources taken from Hardcastle et al., as expected, since we believe that the X-ray emission mechanisms in lobes and hot spots are different.

As part of a study of X-ray emission from jets, hot spots, and lobes, Kataoka & Stawarz (2005) investigated the X-ray emission processes in a sample of 18 previously detected radio lobes. They conclude that IC emission with an equipartition magnetic field is the best model for lobe X-ray emission for their smaller sample, in good agreement with our results. Together with the work we present here, these results provide strong support for the argument that FR II radio lobes are near to equipartition.

To summarize, we find that detectable X-ray emission from the lobes of FR II radio galaxies and quasars is common, that it is due predominantly to IC scattering of CMB photons, and that most FR II sources are close to equipartition, with the energy densities perhaps being electron-dominated by a factor of a few. In the next sections, we discuss reliability issues and alternative explanations of our results.

5. DISCUSSION

5.1. *Reliability Issues*

As discussed in the Appendix, our conclusions in several cases differ significantly from the work of previous authors. It is extremely difficult to obtain a correct flux measurement for lobe-related X-ray emission, because the best choice of extraction regions is sometimes uncertain. It is difficult to avoid AGN contamination, particularly when the radio-lobe emission lies close to the core, and it is also important to exclude any contribution from a hot-gas atmosphere. We have carefully chosen our background regions to be at the same distance from the nucleus as the source regions, although in two cases (3C 200 and 3C 452) this was not possible because the radio-related X-ray emission surrounds the core. We believe that it is the difficulty of correctly separating the different components of the X-ray emission that has led to discrepant results in the literature. It is extremely unlikely that any of our flux measurements are *underestimates* of the lobe IC emission, so that any systematic uncertainty in the R-values is likely to be in the direction of overestimation. As mentioned in § 4, overestimation of R-values may be a particular problem for some of the quasars with strong AGNs and small angular sizes.

5.2. *Assumptions about the Low-Energy Electron Population*

As mentioned in § 1, the properties of the low-energy electron population in the radio lobes are not well constrained, largely due to the lack of instruments capable of measuring the synchrotron emission from this population. This is particularly problematic when studying the IC/CMB process, as it is the low-energy electrons that scatter the CMB to X-ray energies. Since we can-

not use observations to constrain directly the electron energy distribution below 178 MHz for our sample, it is necessary to assume a low-frequency spectral index, δ, and cutoff energy, $\gamma_{\min}$. For this work, we assumed that at low energies, the electron population has an energy index $\delta = 2$, which corresponds to the prediction from shock acceleration. This prediction is supported by observations of hot spots (e.g., Meisenheimer et al. 1997), which have the low-frequency spectral index predicted by the models. We therefore assume that the electron population in the lobes has been shock-accelerated while passing through the hot spots, resulting in an initial energy distribution with $\delta = 2$ (corresponding to a spectral index $\alpha = 0.5$). Spectral aging has then steepened the spectrum at observable frequencies to the observed values of 0.5–1.0. Our modeled energy distribution (§ 3) is therefore a power-law of index 2 at low energies, with a break to a steeper slope in the observable radio region. We also chose to use $\gamma_{\min} = 10$, motivated partly by observations of $\gamma_{\min} \sim 100$–1000 in hot spots (e.g., Carilli et al. 1991)—we would expect a lower $\gamma_{\min}$ in lobes due to the effects of adiabatic expansion—and partly to be conservative. We believe that, given the lack of knowledge about this electron population, our chosen electron energy distribution is physically plausible; however, it is important to consider the effects of varying δ and $\gamma_{\min}$, particularly since the measured X-ray spectral index for those sources where a spectral model could be fitted is steeper than 0.5 in a few cases.

We first tested the effects of varying $\gamma_{\min}$ for several of our sources, covering a range of R-values. If we adopt $\gamma_{\min} = 1000$, corresponding to the lower limit of observed radio emission from lobes, we find new R-values that do not differ from the quoted values (Table 7) for $\gamma_{\min} = 10$ within the $1\,\sigma$ errors. The reason that the prediction for X-ray IC emission does not change significantly is that, while the reduced energy range decreases the electron density, the normalization of the electron energy spectrum increases in order to maintain equipartition.

We next tested the effect of varying δ. An alternative approach to our method is to assume that the electron energy index implied by the low-frequency radio spectral index can be extrapolated back to $\gamma_{\min}$. We tested the effect of this assumption, using the 3CRR spectral index α measured between 178 and 750 MHz (tabulated in Table 1), which is always greater than 0.5, for several of our sources, using $\gamma_{\min} = 10$ and assuming $\delta = 1 + 2\alpha$ and including a break or high-energy cutoff in the spectrum as needed to fit to the radio spectrum, as in our main analysis. We found that for all of the sources this resulted in a *lower* prediction for the X-ray IC flux, increasing the R-values by a factor of ~ 2. The reason for the lower IC prediction in this case is that the equipartition requirement causes the electron energy spectrum normalization to be lowered with respect to the $\delta = 2$ calculation because of the large contribution to the electron energy density made by the additional low-energy electrons. If we adopt $\gamma_{\min} = 1000$ for this analysis, the electron normalization increases again, because of the reduced energy range, so that the resulting R-values are again roughly consistent with those in Table 7. We therefore conclude that uncertainty in the distribution of electrons at low energies introduces at most a factor of 2 uncertainty into our quoted R-values. This corresponds to a factor of 0.7 in $B_{\mathrm{obs}}/B_{\mathrm{eq}}$ and 4 in U_e/U_b.

5.3. *Anisotropic Inverse Compton Emission from a Nuclear Photon Field*

Our analysis for 3C 265 in Appendix A.5 and for 3C 284 (Croston et al. 2004), as well as the analysis of Belsole et al. (2004) for 3C 184, shows that IC scattering of the photon field

from a hidden quasar does not appear to be the dominant X-ray emission mechanism in these sources. As mentioned in Appendix A.5, the X-ray emission from the IC/nuclear process would be brightest toward the nucleus and decrease rapidly with radius; this is not the morphology that is observed. In contrast, the X-ray emission from CMB IC is expected to follow closely the structure of the low-frequency radio emission, which appears to be the case for those sources where the signal-to-noise ratio is sufficiently high to observe the spatial distribution of emission. Our calculations for IC/nuclear (Appendix A.5), in contrast to the work of other authors, assume that the incident photon field is emitting isotropically. The justification for this assumption comes from observations of the infrared emission from narrow- and broad-line objects that show that the infrared properties of the two types of object are the same (Meisenheimer et al. 2001). IC/nuclear emission may be important in some sources in this sample and may help explain the different distributions of narrow- and broad-line objects. 3C 207 (Brunetti et al. 2002) may be an example where this process is important. However, we have shown that CMB IC with a near equipartition magnetic field can account for the majority of the observed X-ray emission in most narrow-line radio galaxies (and, if projection is taken into account, in many broad-line and objects as well); we conclude that in most cases IC/nuclear is not the dominant process.

5.4. *An Alternative Interpretation: Shock-Heated Gas?*

As discussed in the context of our observations of 3C 223 and 3C 284 (Croston et al. 2004), it is also possible that there is hot, shocked gas surrounding the radio lobes of some sources. The emission from such gas could be mistaken for IC emission, as it is difficult to distinguish spectrally between these models due to the small number of counts from most of the lobes. However, in the cases where spectral fitting could be performed, a thermal model was usually a significantly poorer fit to the data. As mentioned above, the lack of a correlation between R and redshift also suggests that the emission is not dominated by such shocked gas, which would be difficult to detect at high redshifts (based on the assumption that most FR II sources reside in groups, as found by Best (2004), and assuming a typical group luminosity of 10^{42} ergs s^{-1}). In addition, many of the sources have radio morphologies similar to 3C 223 and 3C 284 (Croston et al. 2004), for which we argue that highly supersonic expansion is unlikely. These arguments do not rule out some contribution from hot gas. However, the results from 3C 452, where a two-component model could be fitted, show that it is not possible to explain all of the excess X-ray emission above the equipartition prediction by contamination from thermal emission.

As an additional test, we can compare the expected luminosity of shock-heated gas with the observed luminosity in sources where some estimate of the physical conditions in the external medium has been made. We assume a shock-heated shell surrounding the entire lobe. The temperature of the shock-heated gas is unknown, although the evidence from spectral fits, where these are possible, is that it must be high ($\gtrsim 5$ keV). Fortunately *Chandra*'s response to gas hotter than a few keV is only weakly sensitive to temperature, so this does not restrict our ability to carry out these calculations. We make the assumption that the shock-heated material is gas swept up in the radio lobe's expansion, compressed by some compression factor k; then, if the number of particles swept up by the lobe is N and the lobe's volume is V, the mean density of particles in the shell is kN/V. Assuming uniform density, the luminosity from the shocked shell is CN^2k/V, where C is a constant (depending on the luminosity band of interest, the metal abundance of the shocked ma-

terial, and, weakly, on its temperature). The compression factor is unknown, but given the close match of the detected X-rays to the shape of the radio-emitting lobes, it must be significantly greater than 1: application of standard jump conditions would give $k = 4$, while the observed shock around the southern lobe of Cen A (Kraft et al. 2003) corresponds to $k \approx 10$. We have calculated the expected luminosity for shocked shells in several sources for which we have estimates of the group/cluster parameters (e.g., Hardcastle et al. 2002; Croston et al. 2004). In general we find that the expected luminosity for $k > 1$ exceeds the observed luminosity of the lobes; what we observe is too faint to be compressed, swept-up gas. (The exceptions to this rule are sources that are found to lie in reasonably rich environments: for example, $k = 4$ is allowed by the data for 3C 263.) While the results are uncertain because the physical parameters of the environments are poorly constrained, we consider the general incompatibility of this simple model with the observations to be an additional argument against the picture in which the lobe-related X-rays are due to shock-heated thermal material. If supersonic expansion occurred in a small region of the lobe, e.g., around a hot spot, then the expected luminosity from the shocked gas would be lower and could be compatible with the observations. However, in the largest sources with high signal-to-noise ratio detections (e.g., 3C 452), the X-ray emission is not localized in this way, and any emission from shock-heated gas close to hot spots will have been excluded from our analysis. We therefore conclude that this scenario is probably unimportant for the majority of sources in the sample, although it could contribute in some high-R sources where the data quality is insufficient to rule out localized shock heating.

5.5. *Implications for Particle Content*

If the lobes of FR II sources contained an energetically dominant population of relativistic protons (with a high ratio of U_p/U_e), and the energy densities in magnetic field and *particles* were similar, then R would be expected to be typically less than unity. Our results therefore rule out a model where FR II radio lobes have an energetically important proton population and are at equipartition. It is not possible to rule out directly a model in which radio lobes are highly particle-dominated, i.e., where there is an energetically important population of protons giving a total energy density in particles that is an order of magnitude or more higher than that in the magnetic field. However, such a model cannot explain why the measured magnetic field strengths are always close to the value for equipartition between relativistic *electrons* and magnetic field, unless the mechanism for achieving equipartition requires timescales longer than the lobe lifetimes for protons but not electrons. The results of our survey of FR II radio lobes support the conclusions of our earlier papers on smaller samples of sources (Hardcastle et al. 2002; Croston et al. 2004): the presence of an energetically dominant population of protons is unlikely, because it requires that the magnetic field energy density tends to be similar to the electron energy density rather than the conjectured overall energy density in relativistic particles.

6. CONCLUSIONS

Our study of the X-ray emission from the lobes of FR II radio galaxies and quasars has shown that they can be magnetically dominated by at least a factor of 2; however, more than 70% of the sample are at equipartition or electron-dominated. There is a reasonably narrow distribution of R-values, where R is the ratio of observed to predicted emission from CMB IC from

synchrotron-emitting electrons at equipartition. The distribution peaks at $R \sim 2$, which corresponds to magnetic field strengths within 35% of the equipartition value, or electron dominance (U_e/U_b) by a factor of ~ 5. That the distribution is narrow and close to the expectation for equipartition between relativistic electrons and magnetic field shows that an energetically dominant proton population in FR II radio sources is unlikely. The distribution of apparent R-values differs for narrow-line radio galaxies and broad-line objects (broad-line radio galaxies and quasars); this is due in part to projection effects, but it may also be caused by worse systematic uncertainties for more distant objects. We argue that IC scattering of infrared and optical photons from the nucleus is unlikely to be the dominant X-ray emission process in the majority of radio galaxies and quasars, although it may play some role in smaller objects.

APPENDIX

COMPARISON OF RESULTS FOR SOURCES PREVIOUSLY PRESENTED BY OTHER AUTHORS

In this section, we briefly discuss the lobe emission from the individual sources for which previously published results exist and compare our results with those of other authors.

A1. 3C 9

Fabian et al. (2003) discuss the X-ray emission from this source, attributing it to IC scattering of the CMB; however, they do not carry out a detailed calculation and do not separate the X-ray emission from the eastern radio components (likely to be jet-related) and the western lobe, which we analyzed above. Our results are in rough agreement with their less detailed analysis.

A2. 3C 179

Sambruna et al. (2002) discuss the *Chandra* observation of 3C 179 in the context of a survey of jets studied with *HST* and *Chandra*. Their Figure 1 shows a smoothed image of the X-ray emission; however, their choice of gray scale means that the lobe-related emission does not show up in the image, which emphasizes the jet and hot-spot emission. Our $0.5-5.0$ keV image (Fig. 1) excludes higher energy background counts included in their image (which used a larger energy range) and shows clearly an excess of counts associated with both lobes. Sambruna et al. do not mention the presence of this emission.

A3. 3C 207

The *Chandra* observation of 3C 207 was presented by Brunetti et al. (2002). We measured only 25 $0.5-5$ keV counts using background subtraction at the same distance from the nucleus, whereas they were able to fit a spectrum with nine bins. In their discussion of background subtraction they argue that the choice of background region is not important as the *Chandra* background is extremely low; this suggests that they have not subtracted off the component of background from the wings of the PSF, which is important, as can be seen from their smoothed image. They list several reasons why they believe that IC scattering of the CMB is not the dominant process. They argue that no emission is seen from the western lobe, which is of similar radio luminosity and size to the eastern one; however, as the source is of small angular size and the western lobe is dominated by jet emission, it is not possible to obtain a strong upper limit on its lobe-related X-ray emission, particularly in the presence of high background due to AGN emission. Brunetti et al. argue that the X-ray spectral index is flatter than the radio spectral index; however, first, there do not appear to be sufficient counts to constrain the spectral index, and second, they consider only the high-frequency spectral index, whereas it is lower energy electrons that will scatter the CMB and the nuclear emission. We obtained an R-value of 3 for the western lobe of 3C 207 (the intrinsic value may be lower due to projection; see above). It is therefore possible that some contribution to the X-ray flux comes from the IC/nuclear process, as argued by Brunetti et al. (2002), but it appears that CMB IC can explain a significant fraction of the observed emission if the lobe is near equipartition, or all of the X-rays if the lobe is modestly electron-dominated or at a small angle to the line of sight.

A4. 3C 219

Comastri et al. (2003) present the *Chandra* observation of 3C 219 and attribute the lobe-related emission to IC scattering of the CMB and nuclear AGN photons. Our spectral results for the northern lobe are consistent with the values they obtain for the entire source. However, their quoted flux is approximately twice our measured total flux from both lobes. This is probably due to their choice of spectral extraction region, which does not exclude the jet or nothern hot-spot regions. In addition, they do not specify their choice of background region: if it is off-axis, then their spectrum could contain significant AGN contamination. We obtain a comparable flux to their measured value if we use a large elliptical extraction region that includes the jet and northern hot spot, and use an off-source background region. We believe that our choice of extraction regions is preferable, as our regions follow the radio structure more closely, and because our background region, at the same distance from the core as the source regions, will remove contamination from the AGN and hot-gas environment. Therefore, we disagree with their conclusions that the lobes are electron-dominated by up to a factor of 100, and find that this factor is more than an order of magnitude lower.

A5. 3C 265

Bondi et al. (2004) present the results of an analysis of the *Chandra* observation of 3C 265. They interpret the origin of the X-ray emission as IC scattering of AGN photons; however, our results show that CMB and SSC IC emission in an equipartition field can account for more than one-third of the observed X-ray emission. It is nevertheless possible that IC/nuclear scattering makes a significant contribution to the flux from the eastern lobe, thought to be pointing away from us. To test this, we carried out similar calculations for this source to those for the eastern lobe of 3C 284 presented by Croston et al. (2004).

To model the illuminating flux, we used the infrared measurements (at 4.5, 6.7, and 12.0 μm) for 3C 265 of Siebenmorgen et al. (2004), extrapolating to a frequency range of 4×10^{12} to 10^{15} Hz. In order to model the shape of the spectrum at lower frequencies, we scaled the lower frequency spectrum for 3C 295 (Meisenheimer et al. 2001) to a value appropriate for the normalization of 3C 265's infrared spectrum. We used the same parameters for the electron energy spectrum as in the analysis of § 3, with γ_{min} of 10, so that the predicted flux is an upper limit on the IC/nuclear contribution. We find that the contribution to the predicted 1 keV flux density from IC scattering of this photon field to be less than 0.03 nJy for all choices of inclination angle. Therefore, if the infrared emission is isotropic, this process cannot account for the observed flux level. In order to produce the additional X-ray flux (the observed excess of 1.7 nJy above the CMB IC prediction; see Table 7), the luminosity of the quasar as seen by the lobes would have to be $\sim$60 times more luminous than the isotropic luminosity, so that a beam of small opening angle would be required. This more luminous photon field, if symmetric on each side of the source, would also produce a significant flux from the western radio lobe (e.g., $\sim$1 nJy for the most probable angle of 69°), so that IC/nuclear scattering in an equipartition magnetic field cannot explain the observed fluxes. Another argument against illumination from a narrow cone of infrared emission is the lack of evidence for differences in the infrared properties of narrow- and broad-line radio galaxies (Meisenheimer et al. 2001). Finally, the IC/nuclear model predicts a steep decrease in the X-ray flux with distance from the nucleus; this is not seen in the X-ray data. The asymmetry in X-ray to radio flux is therefore more plausibly explained by a difference in the relative magnetic field strength of the two lobes, perhaps due to their different sizes.

There are several differences between our method and that of Bondi et al., which may explain our different conclusions as to the dominant photon population. Our X-ray observational measurements appear to be in reasonable agreement; however, from our *L*-band radio map we measure a much smaller flux ratio between the two lobes than that quoted by Bondi et al. (a ratio of 2.7 between the east and west lobes). We also use a concordance model cosmology, whereas Bondi et al. use a value of $q_0 = 0.5$; this has a significant effect on the volumes and the CMB energy density. The different radio measurements and cosmology may explain why our value for the equipartition magnetic field (2.4 nT) is a factor of 2 below theirs. We used an illuminating spectrum based directly on the infrared measurements of Siebenmorgen et al. (2004) for 3C 265, which gives an integrated luminosity just below the lower limit of the range quoted by Bondi et al. In contrast, they use a value close to the upper limit of their quoted range. Finally, we assumed that the illuminating source is isotropic, as supported by arguments from unified models (see above). We believe our choice of cosmology is more appropriate, and our parametrization of the illuminating source is based directly on infrared measurements, and so we conclude that, in contrast to the findings of Bondi et al., IC from CMB photons in a near-equipartition field ($B \sim 0.6B_{eq}$) can explain the observed X-ray flux, and that the contribution from IC/nuclear is not dominant in this source.

A6. 3C 281

Crawford & Fabian (2003) presented the *Chandra* observation of 3C 281 and attributed the extended X-ray emission to the northern hot spot and environment. They mention the presence of extended soft emission along the jet axis of the four sources they observe in the context of lobe IC emission; however, they concentrated primarily on the environmental properties and did not carry out any analysis of radio-related emission. The emission they considered to be hot spot–related is not sufficiently compact or directly associated with the radio hot spot, leading Hardcastle et al. (2004) to argue that the radio-related emission is associated instead with the lobe. Crawford & Fabian found that the luminosity of the extended emission is much lower than the values estimated using *ROSAT*, which is probably due to the poorly known *ROSAT* PSF. The true group or cluster luminosity may be even lower, once the contribution from lobe-related emission is removed.

A7. 3C 452

An in-depth study of the lobe-related emission from 3C 452 was presented by Isobe et al. (2002), including analysis of the spatial structure of electrons and magnetic field in the lobes. They attribute all of the nonthermal emission to IC scattering of the CMB and find a best-fitting power-law plus Raymond-Smith model with similar spectral parameters to those given in Table 2. They carry a simple comparison of the ratios of synchrotron radiation to X-ray IC emission and estimate that the lobes are electron dominated by a factor of 27^{+25}_{-16}. Their lower limit is roughly consistent with our estimated value of 9, which was determined using a more detailed synchrotron and IC modeling procedure.

REFERENCES

Aldcroft, T. L., Siemiginowska, A., Elvis, M., Mathur, S., Nicastro, F., & Murray, S. S. 2003, ApJ, 597, 751
Barthel, P. D. 1989, ApJ, 336, 606
Bell, A. R. 1978, MNRAS, 182, 147
Belsole, E., Worrall, D. M., Hardcastle, M. J., Birkinshaw, M., & Lawrence, C. R. 2004, MNRAS, 352, 924
Best, P. N. 2004, MNRAS, 351, 70
Bondi, M., Brunetti, G., Comastri, A., & Setti, G. 2003, NewA Rev., 47, 443
———. 2004, MNRAS, 354, L43

Brunetti, G., Bondi, M., Comastri, A., & Setti, G. 2002, A&A, 381, 795
Brunetti, G., Cappi, M., Setti, G., Feretti, L., & Harris, D. E. 2001, A&A, 372, 755
Brunetti, G., Setti, G., & Comastri, A. 1997, A&A, 325, 898
Carilli, C. L., Perley, R. A., Dreher, J. W., & Leahy, J. P. 1991, ApJ, 383, 554
Celotti, A., & Fabian, A. C. 1993, MNRAS, 264, 228
Clarke, D. A., Bridle, A. H., Burns, J. O., Perley, R. A., & Norman, M. L. 1992, ApJ, 385, 173
Comastri, A., Brunetti, G., Dallacasa, D., Bondi, M., Pedani, M., & Setti, G. 2003, MNRAS, 340, L52

Crawford, C. S., & Fabian, A. C. 2003, MNRAS, 339, 1163
Crawford, C. S., Fabian, A. C., Sanders, J. S., & Ettori, S. 2003, NewA Rev., 47, 239
Croston, J. H., Birkinshaw, M., Hardcastle, M. J., & Worrall, D. M. 2004, MNRAS, 353, 879
Dickey, J. M., & Lockman, F. J. 1990, ARA&A, 28, 215
Donahue, M., Daly, R. A., & Horner, D. J. 2003, ApJ, 584, 643
Fabian, A. C., Celotti, A., & Johnstone, R. M. 2003, MNRAS, 338, L7
Fanaroff, B. L., & Riley, J. M. 1974, MNRAS, 167, 31P
Giovannini, G., Feretti, L., Venturi, T., Lara, L., Marcaide, J., Rioja, M., Spangler, S. R., & Wehrle, A. E. 1994, ApJ, 435, 116
Hardcastle, M. J., Birkinshaw, M., Cameron, R. A., Harris, D. E., Looney, L. W., & Worrall, D. M. 2002, ApJ, 581, 948
Hardcastle, M. J., Birkinshaw, M., & Worrall, D. M. 1998a, MNRAS, 294, 615
———. 2001, MNRAS, 323, L17
Hardcastle, M. J., Harris, D. E., Worrall, D. M., & Birkinshaw, M. 2004, ApJ, 612, 729
Hardcastle, M. J., & Worrall, D. M. 2000, MNRAS, 319, 562
Hardcastle, M. J., Worrall, D. M., & Birkinshaw, M. 1998b, MNRAS, 296, 1098
Harris, D. 2005, in ASP Conf. Ser., From Clark Lake to the Long Wavelength Array: Bill Erickson's Radio Science, ed. E. Kassim et al. (San Francsisco: ASP), in press
Homan, D. C., & Wardle, J. F. C. 1999, AJ, 118, 1942
Isobe, N., Tashiro, M., Makishima, K., Iyomoto, N., Suzuki, M., Murakami, M. M., Mori, M., & Abe, K. 2002, ApJ, 580, L111
Kataoka, J., Edwards, P., Georganopoulos, M., Takahara, F., & Wagner, S. 2003a, A&A, 399, 91
Kataoka, J., Leahy, J. P., Edwards, P. G., Kino, M., Takahara, F., Serino, Y., Kawai, N., & Martel, A. R. 2003b, A&A, 410, 833
Kataoka, J., & Stawarz, L. 2005, ApJ, 622, 797
Kino, M., & Takahara, F. 2004, MNRAS, 349, 336
Kraft, R., Hardcastle, M., Worrall, D., & Murray, S. 2005, ApJ, 622, 149
Kraft, R. P., Vázquez, S. E., Forman, W. R., Jones, C., Murray, S. S., Hardcastle, M. J., Worrall, D. M., & Churazov, E. 2003, ApJ, 592, 129
Laing, R. A., Jenkins, C. R., Wall, J. V., & Unger, S. W. 1994, in ASP Conf. Ser. 54, The First Stromlo Symposium: The Physics of Active Galaxies, ed. G. V. Bicknell, M. A. Dopita, & P. J. Quinn (San Francisco: ASP), 201
Leahy, J. P., Bridle, A. H., & Ström, R. G. 1998, An Atlas of DRAGNs (Manchester: Univ. Manchester), http://www.jb.man.ac.uk/atlas/index.html
Leahy, J. P., & Perley, R. A. 1991, AJ 102, 537
———. 1995, MNRAS, 277, 1097
Liu, R., & Pooley, G. 1991, MNRAS, 249, 343
Meisenheimer, K., Haas, M., Müller, S. A. H., Chini, R., Klaas, U., & Lemke, D. 2001, A&A, 372, 719
Meisenheimer, K., Yates, M. G., & Roeser, H.-J. 1997, A&A, 325, 57
Overzier, R., Harris, D., Carilli, C., Pentericci, L., Röttgering, H., & Miley, G. 2005, A&A, 433, 870
Reynolds, C. S., Brenneman, L. W., & Stocke, J. T. 2005, MNRAS, 367, 381
Sambruna, R. M., Maraschi, L., Tavecchio, F., Urry, C. M., Cheung, C. C., Chartas, G., Scarpa, R., & Gambill, J. K. 2002, ApJ, 571, 206
Siebenmorgen, R., Freudling, W., Krügel, E., & Haas, M. 2004, A&A, 421, 129
Urry, C. M., & Padovani, P. 1995, PASP, 107, 803
Wardle, J. F. C., Homan, D. C., Ojha, R., & Roberts, D. H. 1998, Nature, 395, 457
Wilson, A. S., Young, A. J., & Shopbell, P. L. 2000, ApJ, 544, L27
Worrall, D. M., Birkinshaw, M., Hardcastle, M. J., & Lawrence, C. R. 2001, MNRAS, 326, 1127